HHS Public Access

Author manuscript

Lab Chip. Author manuscript; available in PMC 2018 August 08.

Published in final edited form as:

Lab Chip. 2017 August 08; 17(16): 2805–2813. doi:10.1039/c7lc00668c.

Robust Manufacturing of Lipid-Polymer Nanoparticles through Feedback Control of Parallelized Swirling Microvortices

Michael J. Toth[a], **Taeyoung Kim**[a], and **YongTae Kim**[a,b,c,d,*]

[a]George W. Woodruff School of Mechanical Engineering, Georgia Institute of Technology, Atlanta, Georgia 30332, USA

[b]Wallace H. Coulter Department of Biomedical Engineering, Georgia Institute of Technology, Atlanta, Georgia 30332, USA

[c]Parker H. Petit Institute for Bioengineering and Bioscience, Georgia Institute of Technology, Atlanta, Georgia 30332, USA

[d]Institute for Electronics and Nanotechnology, Georgia Institute of Technology, Atlanta, Georgia 30332, USA

Abstract

A variety of therapeutic and/or diagnostic nanoparticles (NPs), or nanomedicines, have been formulated for improved drug delivery and imaging applications. Microfluidic technology enables continuous and highly reproducible synthesis of NPs through controlled mixing processes at the micro- and nanoscale. Yet, the inherent low-throughput remains a critical roadblock, precluding the probable applications of new nanomedicines for clinical translation. Here we present robust manufacturing of lipid-polymer NPs (LPNPs) through feedback controlled operation of parallelized swirling microvortex reactors (SMRs). We demonstrate the capability of a single SMR to continuously produce multicomponent NPs and the high-throughput performance of parallelized SMRs for large-scale production (1.8kg/d) of LPNPs while maintaining the physicochemical properties. Finally, we present robust and reliable manufacturing of NPs by integrating the parallelized SMR platform with our custom high-precision feedback control system that addresses unpredictable disturbances during the production. Our approach may contribute to efficient development and optimization of a wide range of multicomponent NPs for medical imaging and drug delivery, ultimately facilitating good manufacturing practice (GMP) production and accelerating the clinical translation.

Graphical abstract

*Corresponding author: YongTae Kim, George W. Woodruff School of Mechanical Engineering, Georgia Institute of Technology, 345 Ferst Drive (Rm 3134), Atlanta, GA 30332, (phone) 404-385-1478, (fax) 404-385-8535, ytkim@gatech.edu.

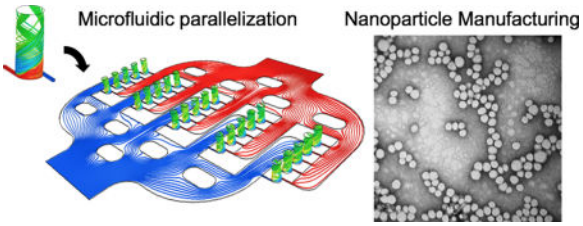

Keywords

microfluidics; nanoparticle; functionalization; high-throughput; parallelization; large-scale; multifunctional

Introduction

A number of nanomedicines have been developed for targeted delivery of therapeutic and imaging agents for the treatment and diagnosis of major diseases including cancer,[1–3] cardiovascular disease,[4–5] diabetes,[6–7] and Alzheimer's disease.[8–10] More than 30,000 research articles are annually reported to show the development of novel nanomedicines for potential treatment of several fatal diseases; however, a few candidates are successfully validated for clinical trials. For a decade, only a small number of therapeutic and diagnostic (theranostic) NPs have been approved by the FDA.[11–12] This low success rate in the "bench to bedside" translation is due in part to low reproducibility of desired properties or efficacies of developed nanomedicines in prescreening processes from in vitro testing to in vivo validation.[13] With pharmaceutical and biomedical industries acknowledging the challenges in scaling the production of NPs, there is a growing need for the development of robust technology for nanomedicine manufacturing.[14–16]

Microfluidic platforms provide controllable flow patterns with tunable characteristic mixing times on the millisecond to microsecond scale that can be used for diffusive or convective mixing mechanisms.[17–25] Numerous studies have demonstrated that microfluidic synthesis produces narrower NP size distributions (i.e., high size uniformity) than those of conventional multi-step benchtop synthesis methods,[26–27] but the production rate remains restricted by a low throughput (up to a few grams per hour).[28–29] A recent approach using a turbulent impinging jet flow to synthesize polymeric NPs in a single device achieved a much higher production rate on the order of kg/d;[30] however, optimization process of multicomponent NP synthesis in turbulent flow at macroscale remains impractical due to waste of costly precursors, and the effect of the high shear rate generated by turbulent flow on the stability or degradation of precursors remains to be investigated. This challenge underscores the importance of microfluidic parallelization technology that preserves the advantages of the microscale reaction by maintaining the characteristic mixing times on the millisecond to microsecond scale and the consistency of reactor conditions. Although several microfluidic parallelization approaches have been previously introduced using simple diffusive mixing to improve production rates from mg/d to g/d,[15, 31–33] no reliable and practical approach has been established for scalable manufacturing of NPs to an industrially relevant level, such as attaining a production rate on the order of kg/d.[12, 15, 34–36]

Here we present a parallelized microfluidic platform integrated with feedback control designed to demonstrate robust manufacturing of multicomponent NPs with the controlled physicochemical properties. We first describe a design and optimization process of a simple SMR for continuous and highly reproducible synthesis of LPNPs and then demonstrate the importance of feedback pressure control system to maintain the produced NP size uniformity. Through computational simulations and experimental evaluation of microfluidic flows and pressure profiles, we parallelize SMRs for large-scale production (1.8kg/d) of LPNPs with the controlled physicochemical properties. Finally, we present robust manufacturing of LPNPs with feedback control of parallelized SMRs.

RESULTS and DISCUSSION

Swirling Microvortex Reactor

We developed a swirling microvortex reactor (SMR) by modelling and tuning the mixing efficiency, a predictive measure of reaction conditions empirically linked to NP size uniformity (Fig. 1a). We used computational fluid dynamics (CFD) simulations to achieve a 90% or higher mixing efficiency with varied SMR diameters (Fig. 1b and Fig. S1). We determined that the mixing efficiency of SMRs with diameters of 1mm, 2mm, and 4mm have characteristic mixing times (4ms, 16ms, and 64ms, respectively) less than the residence time (20ms, 40ms, and 80ms, respectively) of the reactor when the height is held constant at 5mm. With the tuned SMR, we were able to continuously produce highly reproducible Lipid-polymer NPs (LPNPs) with high size uniformity at a rate of 3g/h (Fig. 1c and d). LPNPs combine the unique strengths of liposomal and polymeric nanoparticles while overcoming their limitations in terms of drug encapsulation efficiency and storage stability.[37–38] We validated our simulations by synthesizing LPNPs in the SMRs with various diameters (1mm, 2mm, and 4mm) at a constant Reynolds number (Re) of 250, a transitional boundary above which swirling vortex flow patterns become chaotic. With the 2mm diameter, we obtained the highest mixing efficiency (0.92, volumetric average in a SMR) and thus the narrowest size distribution (Fig. 1e) in our synthesis validation. We were also able to demonstrate fine control of the precursor composition (Fig. 1f) and the ability to control the size simply by varying flow rates (i.e., Reynolds numbers (Re)) without changing the precursor composition (Fig. 1g).

Uniform NP Synthesis with High-precision Pressure Control

To produce NPs with high reproducibility, we integrated the SMR with our custom high-precision, feedback pressure control system.[39] We first decomposed the SMR into equivalent resistances and constructed a fluidic circuit analog of the coupled system with both inlets (Fig. 2a). From the equation for Reynolds number,[40–41] the SMR inlet pressure is given as below.

$$P=\frac{[R_1+2R_2]\,\mu A}{2\rho D_H}.Re$$

where μ represents the dynamic viscosity, A represents the cross-sectional area of the SMR, ρ represents the fluid density, D_H represents the hydrodynamic diameter, and Re represents

the Reynolds number. We used this equation to calculate the pressure range corresponding to the Reynolds numbers designed in this study (Fig. 2b). Our control system demonstrated the performance with less than a 0.3 second settling time is maintained across the Reynolds numbers (inlet pressures; Fig. 2c). We also compared the performance of our control system with that of a widely used, commercially available syringe pump; our system showed a 50 times faster transient response (Fig. 2d) and more stable in long-term regulation of a flow rate (Fig. 2e).

With this superior performance of our high-precision control system, we assessed the size uniformity of NPs synthesized on the SMR by comparing the size distributions and the polydispersity index (PDI), a measure of the homogeneity of the size distributions. LPNPs produced on the SMR using our pressure control system showed narrower size distributions than those using a syringe pump for steady-state (long-term) (Fig. 2f and g) and transient (short-term) performance (Fig. 2h and i). The difference in the NP distributions and PDI values from the steady-state response is because feedback pressure control system rejects external disturbances and minimizes the variation in the inlet pressure of the SMR (Fig. 2f and g). This disturbance rejection preserves the Reynolds number and precursor composition, which are two critical factors that affect NP physicochemical properties. The difference in the NP distributions from the transient response is because it takes longer (settling time upwards of minutes)[42–43] for the syringe pump to reach steady-state values than for our control system (less than 0.3 second settling time response) (Fig. 2h and i).

SMR integration for parallelized microvortex array (PMA)

To engineer a parallelized array of tuned SMRs, we reduced the local pressure and flow variations of our microfluidic network and identified the number of tunable variables to scale the PMA (Fig. 3a). To maintain the same physicochemical properties of produced NPs, we need to reduce SMR-SMR reaction variations in the PMA, which are critical NP synthesis parameters affecting NP property uniformity to ensure reaction consistency across a plurality of SMR. We employed a fluidic circuit analog[44] to optimize the PMA inlet fluidic impedances (Z_1 and Z_2) given the SMR inlet impedances (Z_3 and Z_4) (Fig. 3b). Each fluidic impedance consists of the fluidic resistance R and capacitance C. To minimize pressure variations at the inlet of each SMR in the PMA, the microfluidic channels networking the SMRs should lead to an identical pressure drop between the pressure source and the inlet of each SMR. This methodology is accomplished by equating the Hagan-Poiseuille equation for fluidic systems with Ohm's Law for electrical circuits. This is based on the assumption of an incompressible Newtonian fluid in laminar flow. In our microfluidic channel hierarchy (Fig. 3b), we found that the Z_2:Z_3 ratio is a key design parameter to be tuned to minimize pressure variations at the inlet of each SMR in the PMA. To determine a desired Z_2:Z_3 ratio, we assessed the flow rate ratio between the inlets of the first and last SMR within a PMA column and found that an increase in the array size (i.e., the number of the tuned SMR in a PMA) requires a decrease in Z_2:Z_3 ratio to maintain the same flow rate ratio. More importantly, the flow rate ratio in a larger array size is more sensitive to the variations in the Z_2:Z_3 impedance ratio, requiring a higher accuracy for fabrication in a larger PMA. In the current platform of 5×5 array, we utilized a flow rate ratio (0.92) resulting in a Z_2:Z_3 ratio (0.021) (Fig. S2).

We then used CFD simulations to further tune this electrical PMA model by minimizing local flow variations across the initial (Fig. 3c) and tuned fluidic (Fig. 3d) models, finalizing the PMA design with less than 1% precursor composition variation and less than 4% Re variation (Fig. 3e). This refinement of our PMA model simulated with the best PLGA-to-lipid weight ratio of 5 and the best Re of 250 decreased the variation of the precursor composition at the inlet of each SMR in the PMA by 79.4% (Fig. 3f) and improved the mixing consistency across the SMRs by 1.5% (Fig. 3f) and across the height of the SMR (Fig. 3h). While the average mixing efficiency in the outlet of the PMA (91%) was lower than that of the tuned SMR (98%) (Fig. 2a), the difference was not significant as a mixing efficiency above 90% showed comparable NP size distribution in our experimental data (Fig. 1e–g). The fabricated PMA device with two inlets for precursor solutions and one outlet for NPs (Fig. 3i) consists of a multitier platform: a parallelized microvortex network for connecting all 25 SMRs, microvortex reactors for rapidly mixing precursors for NP synthesis, and a collection reservoir to create a common outlet for all the SMRs with all layers interlaced with gaskets to prevent leakages (Fig. 3j). Our designed PMA model achieved a 25-fold greater production rate of LPNPs while maintaining the size distributions similar to those synthesized using the tuned SMR (Fig. 3k).

Robust manufacturing with feedback control

In addition to reducing SMR-to-SMR variation of critical reaction parameters, we need to mitigate inlet flow variations in the PMA, a factor that amplifies designed parameter variations. We coupled our PMA with a high-precision, feedback pressure control system to regulate the inlet pressure of the PMA while mitigating external disturbances and reducing precursor flow fluctuations (Fig. 4a). The feedback pressure control system demonstrated the performance with less than a 0.3 second settling time (Fig. 4b), and maintained long-term experimentation (greater than 3 hours) (Fig. 4c) while mitigating pressure fluctuations within a 0.5% absolute error (Fig. 4d). To demonstrate the advantage of coupling our feedback control system, we compared the production of LPNPs with and without the control in response to an external disturbance (Fig. 4e). Without the mitigation of flow fluctuations, the NP size uniformity is substantially reduced. The integration of the PMA with the feedback control provides not only highly reproducible uniform LPNP production for long-term duration but also mitigates external disturbances that would otherwise cause a failure to achieve robust manufacturing.

Conclusions

We have presented a representative example for robust manufacturing (1.8kg/d) of multicomponent NPs through feedback controlled, parallelized microfluidic reactors. Our parallelized reactor design can be further extended to a larger array, achieving a greater production rate that addresses the current manufacturing challenges that pharmaceutical and biomedical industries face. The integration of advanced microfluidic technology with control systems engineering may validate a new impactful method for robust NP manufacturing and contribute to efficient development and optimization of a wide range of multicomponent NPs for therapeutic and diagnostic applications.

Methods and Materials

Microfluidic device design and fabrication

The PMA device was fabricated out of UNS S30400 stainless steel (McMaster Carr, Chicago IL) with a computerized numerical control (CNC; the Haas OM-1a) machine at 30,000 rpm to micro-machine the SMR channels. The stainless steel allows for good chemical resistance allowing for robust synthesis applications while providing a high Young's modulus to resist deformation under high pressure, which would otherwise lead to possible flow dynamic disruption. To prevent leakages between the 3-component system, custom gaskets of ethylene propylene diene monomer (EPDM) rubber (Ponn Machine Cutting Company, Woburn, MA) were designed. To ensure the device could handle high pressure sources (>200 psi), the inlet and outlet push-to-connect fittings were rated in excess of 250 psi. The 3 components were radially compressed with 25 in-lb torque on 8–1/4 in bolts.

Fluidic Circuit Analog

To initially model the PMA, the microfluidic channel hierarchy was decomposed by fluidic resistance R_{rect} or R_{cir}, and fluidic capacitance, C. The parallel circuit schematic can be combined into a singular equation, Z_i, representing the microfluidic impedance, where s represents the complex variable of the Laplace transform. The equations for the mentioned parameters are as follows:

$$R_{rect}=\frac{12\mu L}{wh^3\left(1-\frac{0.63h}{w}\right)}$$

$$R_{cir}=\frac{8\mu L}{\pi r^4}$$

$$C=\frac{V}{P}$$

$$Z_i=\frac{R_i}{R_iC_is+1}$$

where μ represents the dynamic viscosity, L represents the channel length, w and h represent width and height, respectively, of a rectangular cross-section, and r represents radius of a circular channel. Capacitance, C, is defined as the total volume, V, over the pressure, P.

The minimization of the Z_2:Z_3 ratio was to maintain a flow rate ratio of 0.9 between the first and last SMR within a set (Table 1). As the size of the array increases, the Z_2:Z_3 ratio must decrease to maintain the ratio by either increasing the width and/or length of Z_2. The 5×5

array chosen is located close to the asymptote of the graph, indicating further increases in array dimensions do not greatly impact the required Z_2:Z_3 ratio. However, when we look at the sensitivity of the array to changes in the Z_2:Z_3 ratio, the larger the dimensional array the more sensitive the flow rate ratio. The increased sensitivity indicates larger dimensional arrays will need to have a higher precision of fabrication to achieve designed flow rate ratios, which may present a challenge when micromachining. The model developed here was a 5×5 array utilizing a Z_2:Z_3 ratio of 0.021 to achieve a flow rate ratio of 0.92.

Mixing efficiency

To computationally analyze the SMR and PMA platforms, we developed a simple mixing efficiency model by weighting the mass fraction based on a continuous linear piecewise function where a mass fraction of 0.5 correlates to a mixing efficiency of 1 (Fig. S3).

$$Mix_{eff} = \begin{cases} 2.Mass_{fract}, & Mass_{fract} \leq 0.5 \\ 2 - 2.Mass_{fract}, & Mass_{fract} > 0.5 \end{cases}$$

The evaluation of potential effectiveness of microfluidic devices may be assessed by the cross sectional and volumetric evaluation of the mixing efficiency. The mixing efficiency values reported were obtained by integrating over cross-sectional planes of both the SMR and PMA reactors, creating an average mixing efficiency, at 0.5, 1.5, 2.5, 3.5, and 4.5 mm in height.

$$Mix_{eff\_ave} = \frac{\iint Mix_{eff} dA}{\iint dA}$$

Numerical simulations

Numerical simulations of the fluid dynamics were calculated using a commercial CFD solver (SC/Tetra, Cradle North America Inc., Beavercreek, OH). The advection-diffusion of chemical species was solved, with a diffusivity constant of 1e-9 m^2/s, to calculate mass fraction and mixing efficiency. The models assumed a Newtonian fluid at room temperature (25°C) with a no-slip boundary condition at the walls. Flow rates were specified at the two inlets with an outlet condition of atmospheric pressure.

NP Synthesis

Polymer (Poly(lactic-co-glycolic acid) (50:50) (PLGA); 30~60kDA) was obtained from Sigma Aldrich (St. Louis, MO) and lipids (1,2-distearoyl-sn-glycero-3-phosphoethanolamine-N-[amino(polyethylene glycol)-2000] (DSPE-PEG) and 1,2-dipalmitoyl-sn-glycero-3-phosphocholine (DPPC)) were obtained from Avanti Polar Lipids (Alabaster, AL). LPNPs were synthesized by rapidly mixing a solution of PLGA in acetonitrile with a solution of DSPE-PEG and DPPC, in a 7:3 DPPC to DSPE-PEG molar ratio, in 4% ethanol at a Re of 250 in the SMR. LPNPs were purified by triplicate centrifugal filtration with a 30 kDA filter (EMD Millipore Corp, Darmstadt, Germany) at 2900 rpm for 15 minutes.

Production rate calculation

The production rate for the SMR and PMA platforms was calculated by:

$$\text{Production Rate}\,(\text{total wt/h}) = (C_1 + C_2) \cdot Q$$

where C_1 and C_2 represent the concentrations of PLGA (3.75 mg/mL) and lipid solution (0.15 mg/mL) respectively. Because the flow rate to both the SMR and PMA are symmetric at each inlet, Q represents the flow rate of 1 inlet to the microfluidic device; 11.8 mL/min for SMR and 295 mL/min for PMA. The resulting production rate was reported as kg/d.

Nanoparticle morphology visualization

Samples were imaged by transmission electron microscopy (TEM; JEOL 100 CX-II) at a voltage of 100 kV. LPNP samples were prepared by depositing 10 μL of NP solution on a 200-mesh formvar coated copper grid (Electron Microscopy Sciences, Hatfield, PA). The samples were dried for 30 minutes before blotting away the remaining solution. The NP solutions were then negatively stained with a filtered 2% uranyl acetate solution for 30 seconds. The grids were washed with double distilled water and air-dried for 2 hours prior to imaging.

Disturbance profile

The synthesis of LPNPs on the PMA was disrupted by a decrease in pressure to the lipid precursor (Fig. S4), reducing the lipid inlet flow rate. This disruption was simply designed to cause the LPNP precursor composition to shift above the designed value of 5, causing an increase in the size and decreasing the homogeneity of the synthesis.

Statistical analysis

Significance was determined by an analysis of variance (ANOVA) with an alpha value of 0.05. Multiple comparisons were corrected by the Tukey-Kramer method. The PMA model analysis utilized a two-way ANOVA to compare the two family with three comparisons per family. Comparison of calculated PDI values of SMR synthesized LPNPs with syringe pump and pressure control system utilized a two-tailed Student’s t-test with an alpha of 0.5.

Supplementary Material

Refer to Web version on PubMed Central for supplementary material.

Acknowledgments

This work was supported by the American Heart Association Scientist Development Grant (15SDG25080314), the National Institute of Neurological Disorders and Stroke of the National Institutes of Health (R21NS091682), and the startup resources of Georgia Institute of Technology. This work was in part performed at the Georgia Tech Institute for Electronics and Nanotechnology, a member of the National Nanotechnology Coordinated Infrastructure, which is supported by the National Science Foundation (Grant ECCS1542174). We thank M. Toth and J. Toth for providing the insight into the device design and fabrication.

References

1. Wang AZ, Langer R, Farokhzad OC. Nanoparticle delivery of cancer drugs. Annual review of medicine. 2012; 63:185–198.
2. Davis ME, Shin DM. Nanoparticle therapeutics: an emerging treatment modality for cancer. Nature reviews Drug discovery. 2008; 7(9):771–782. [PubMed: 18758474]
3. Bazak R, Houri M, El Achy S, Kamel S, Refaat T. Cancer active targeting by nanoparticles: a comprehensive review of literature. Journal of cancer research and clinical oncology. 2015; 141(5): 769–784. [PubMed: 25005786]
4. Chung BL, Toth MJ, Kamaly N, Sei YJ, Becraft J, Mulder WJ, Fayad ZA, Farokhzad OC, Kim Y, Langer R. Nanomedicines for endothelial disorders. Nano Today. 2016
5. Donaldson K, Duffin R, Langrish JP, Miller MR, Mills NL, Poland CA, Raftis J, Shah A, Shaw CA, Newby DE. Nanoparticles and the cardiovascular system: a critical review. Nanomedicine. 2013; 8(3):403–423. [PubMed: 23477334]
6. Veiseh O, Tang BC, Whitehead KA, Anderson DG, Langer R. Managing diabetes with nanomedicine: challenges and opportunities Nature Reviews Drug. Discovery. 2015; 14(1):45–57.
7. Sharma G, Sharma AR, Nam J-S, Doss GP, Lee S-S, Chakraborty C. Nanoparticle based insulin delivery system: the next generation efficient therapy for Type 1 diabetes. Journal of nanobiotechnology. 2015; 13(1):74. [PubMed: 26498972]
8. Huang M, Hu M, Song Q, Song H, Huang J, Gu X, Wang X, Chen J, Kang T, Feng X. GM1-Modified Lipoprotein-like Nanoparticle: Multifunctional Nanoplatform for the Combination Therapy of Alzheimer's Disease. ACS nano. 2015; 9(11):10801–10816. [PubMed: 26440073]
9. Muntimadugu E, Dhommati R, Jain A, Challa VGS, Shaheen M, Khan W. Intranasal delivery of nanoparticle encapsulated tarenflurbil: A potential brain targeting strategy for Alzheimer's disease. European Journal of Pharmaceutical Sciences. 2016
10. Gao N, Sun H, Dong K, Ren J, Qu X. Gold-Nanoparticle-Based Multifunctional Amyloid-β Inhibitor against Alzheimer's Disease. Chemistry–A European Journal. 2015; 21(2):829–835.
11. Bobo D, Robinson KJ, Islam J, Thurecht KJ, Corrie SR. Nanoparticle-Based Medicines: A Review of FDA-Approved Materials and Clinical Trials to Date. Pharmaceutical research. 2016:1–15.
12. Chan HF, Ma S, Leong KW. Can microfluidics address biomanufacturing challenges in drug/gene/cell therapies? Regenerative biomaterials. 2016:rbw009.
13. Desai N. Challenges in development of nanoparticle-based therapeutics. The AAPS journal. 2012; 14(2):282–295. [PubMed: 22407288]
14. Valencia PM, Farokhzad OC, Karnik R, Langer R. Microfluidic technologies for accelerating the clinical translation of nanoparticles. Nature nanotechnology. 2012; 7(10):623–629.
15. Lim J-M, Bertrand N, Valencia PM, Rhee M, Langer R, Jon S, Farokhzad OC, Karnik R. Parallel microfluidic synthesis of size-tunable polymeric nanoparticles using 3D flow focusing towards in vivo study. Nanomedicine: Nanotechnology, Biology and Medicine. 2014; 10(2):401–409.
16. Liu D, Cito S, Zhang Y, Wang CF, Sikanen TM, Santos HA. A versatile and robust microfluidic platform toward high throughput synthesis of homogeneous nanoparticles with tunable properties. Advanced Materials. 2015; 27(14):2298–2304. [PubMed: 25684077]
17. Rhee M, Valencia PM, Rodriguez MI, Langer R, Farokhzad OC, Karnik R. Synthesis of Size-Tunable Polymeric Nanoparticles Enabled by 3D Hydrodynamic Flow Focusing in Single-Layer Microchannels. Advanced Materials. 2011; 23(12):H79–H83. [PubMed: 21433105]
18. Sun J, Xianyu Y, Li M, Liu W, Zhang L, Liu D, Liu C, Hu G, Jiang X. A microfluidic origami chip for synthesis of functionalized polymeric nanoparticles. Nanoscale. 2013; 5(12):5262–5265. [PubMed: 23652785]
19. Sun J, Zhang L, Wang J, Feng Q, Liu D, Yin Q, Xu D, Wei Y, Ding B, Shi X. Tunable rigidity of (polymeric core)–(lipid shell) nanoparticles for regulated cellular uptake. Advanced Materials. 2015; 27(8):1402–1407. [PubMed: 25529120]
20. Othman R, Vladisavljević GT, Bandulasena HH, Nagy ZK. Production of polymeric nanoparticles by micromixing in a co-flow microfluidic glass capillary device. Chemical Engineering Journal. 2015; 280:316–329.

21. Zhigaltsev IV, Belliveau N, Hafez I, Leung AK, Huft J, Hansen C, Cullis PR. Bottom-up design and synthesis of limit size lipid nanoparticle systems with aqueous and triglyceride cores using millisecond microfluidic mixing. Langmuir : the ACS journal of surfaces and colloids. 2012; 28(7):3633–3640. [PubMed: 22268499]
22. Mizuno M, Toyota T, Konishi M, Kageyama Y, Yamada M, Seki M. Formation of monodisperse hierarchical lipid particles utilizing microfluidic droplets in a nonequilibrium state. Langmuir : the ACS journal of surfaces and colloids. 2015; 31(8):2334–2341. [PubMed: 25669326]
23. Kim Y, Lee Chung B, Ma M, Mulder WJ, Fayad ZA, Farokhzad OC, Langer R. Mass production and size control of lipid–polymer hybrid nanoparticles through controlled microvortices. Nano letters. 2012; 12(7):3587–3591. [PubMed: 22716029]
24. Kim Y, Fay F, Cormode DP, Sanchez-Gaytan BL, Tang J, Hennessy EJ, Ma M, Moore K, Farokhzad OC, Fisher EA, Mulder WJ, Langer R, Fayad ZA. Single step reconstitution of multifunctional high-density lipoprotein-derived nanomaterials using microfluidics. ACS nano. 2013; 7(11):9975–83. [PubMed: 24079940]
25. Kim, Y., Langer, R. Microfluidics in nanomedicine. In: Meyers, RA., editor. Reviews in Cell Biology and Molecular Medicine. Vol. 1. Wiley-VCH Verlag GmbH & Co.; KGaA: 2015. p. 127-152.
26. Mieszawska AJ, Kim Y, Gianella A, van Rooy I, Priem B, Labarre MP, Ozcan C, Cormode DP, Petrov A, Langer R, Farokhzad OC, Fayad ZA, Mulder WJ. Synthesis of polymer-lipid nanoparticles for image-guided delivery of dual modality therapy. Bioconjugate chemistry. 2013; 24(9):1429–34. [PubMed: 23957728]
27. Hornig S, Heinze T, Becer CR, Schubert US. Synthetic polymeric nanoparticles by nanoprecipitation. Journal of materials chemistry. 2009; 19(23):3838–3840.
28. Sollier E, Murray C, Maoddi P, Di Carlo D. Rapid prototyping polymers for microfluidic devices and high pressure injections. Lab on a chip. 2011; 11(22):3752–3765. [PubMed: 21979377]
29. Fang RH, Chen KN, Aryal S, Hu C-MJ, Zhang K, Zhang L. Large-scale synthesis of lipid–polymer hybrid nanoparticles using a multi-inlet vortex reactor. Langmuir : the ACS journal of surfaces and colloids. 2012; 28(39):13824–13829. [PubMed: 22950917]
30. Lim J-M, Swami A, Gilson LM, Chopra S, Choi S, Wu J, Langer R, Karnik R, Farokhzad OC. Ultra-high throughput synthesis of nanoparticles with homogeneous size distribution using a coaxial turbulent jet mixer. ACS nano. 2014; 8(6):6056–6065. [PubMed: 24824296]
31. Nisisako T, Torii T. Microfluidic large-scale integration on a chip for mass production of monodisperse droplets and particles. Lab on a chip. 2008; 8(2):287–293. [PubMed: 18231668]
32. Romanowsky MB, Abate AR, Rotem A, Holtze C, Weitz DA. High throughput production of single core double emulsions in a parallelized microfluidic device. Lab on a chip. 2012; 12(4): 802–807. [PubMed: 22222423]
33. Mulligan MK, Rothstein JP. Scale-up and control of droplet production in coupled microfluidic flow-focusing geometries. Microfluidics and nanofluidics. 2012; 13(1):65–73.
34. Vladisavljevic GT, Khalid N, Neves MA, Kuroiwa T, Nakajima M, Uemura K, Ichikawa S, Kobayashi I. Industrial lab-on-a-chip: design, applications and scale-up for drug discovery and delivery. Advanced drug delivery reviews. 2013; 65(11–12):1626–63. [PubMed: 23899864]
35. Belliveau NM, Huft J, Lin PJ, Chen S, Leung AK, Leaver TJ, Wild AW, Lee JB, Taylor RJ, Tam YK. Microfluidic synthesis of highly potent limit-size lipid nanoparticles for in vivo delivery of siRNA. Molecular Therapy—Nucleic Acids. 2012; 1(8):e37. [PubMed: 23344179]
36. Hood RR, DeVoe DL. High-Throughput Continuous Flow Production of Nanoscale Liposomes by Microfluidic Vertical Flow Focusing. small. 2015; 11(43):5790–5799. [PubMed: 26395346]
37. Zhao CX, Middelberg AP. Synthesis and Characterization of Nanomaterials Using Microfluidic Technology. Handbook of Nanoparticles. 2016:455–473.
38. Kumari A, Yadav SK, Yadav SC. Biodegradable polymeric nanoparticles based drug delivery systems. Colloids and Surfaces B: Biointerfaces. 2010; 75(1):1–18. [PubMed: 19782542]
39. Kim Y, LeDuc P, Messner W. Modeling and control of a nonlinear mechanism for high performance microfluidic systems. Control Systems Technology, IEEE Transactions on. 2013; 21(1):203–211.

40. Brody JP, Yager P, Goldstein RE, Austin RH. Biotechnology at low Reynolds numbers. Biophysical journal. 1996; 71(6):3430–3441. [PubMed: 8968612]

41. Squires TM, Quake SR. Microfluidics: Fluid physics at the nanoliter scale. Reviews of modern physics. 2005; 77(3):977.

42. Stone HA, Stroock AD, Ajdari A. Engineering flows in small devices: microfluidics toward a lab-on-a-chip. Annu Rev Fluid Mech. 2004; 36:381–411.

43. Martin M, Blu G, Eon C, Guiochon G. The use of syringe-type pumps in liquid chromatography in order to achieve a constant flow-rate. Journal of Chromatography A. 1975; 112:399–414.

44. Oh KW, Lee K, Ahn B, Furlani EP. Design of pressure-driven microfluidic networks using electric circuit analogy. Lab on a Chip. 2012; 12(3):515–545. [PubMed: 22179505]

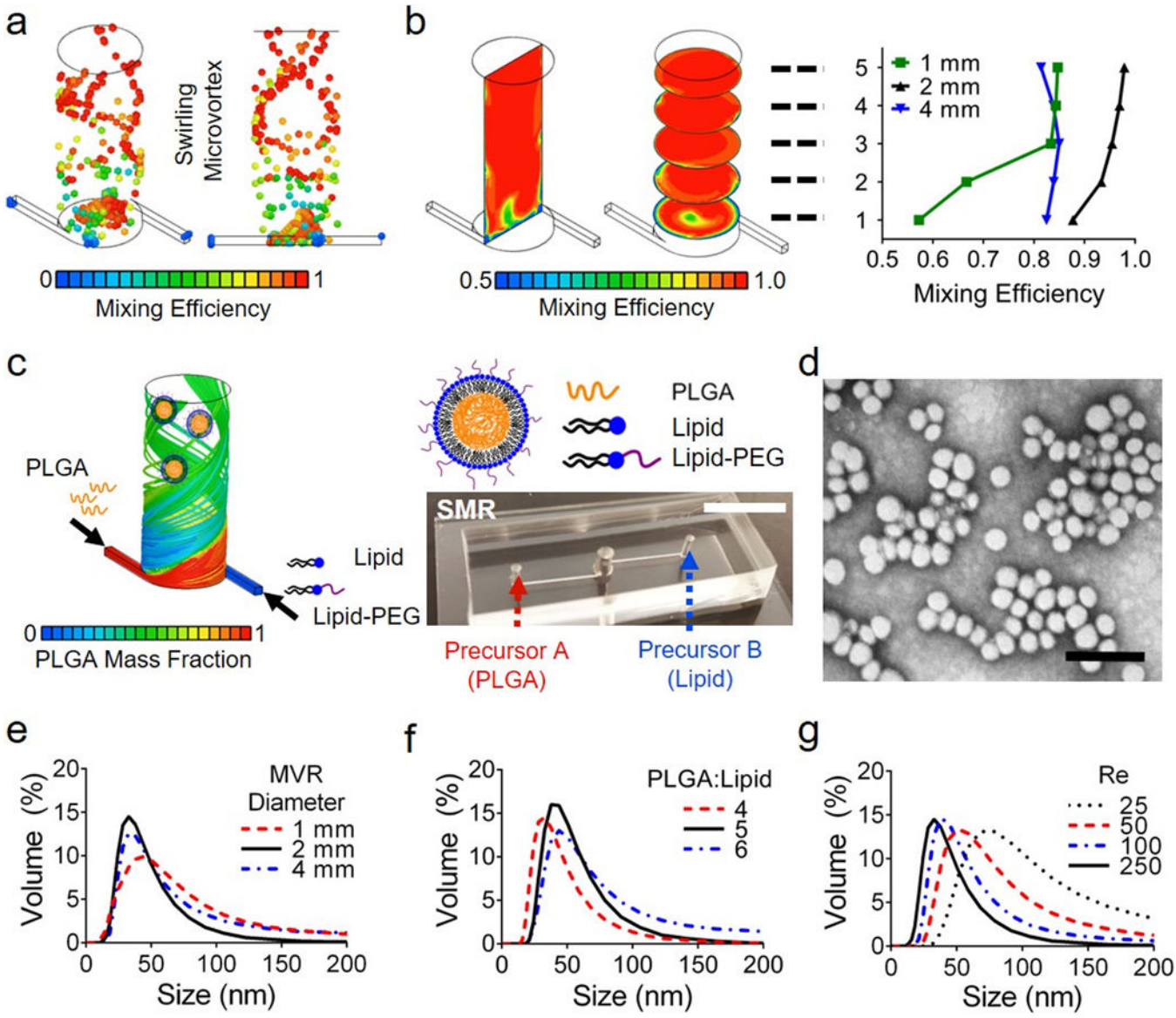

Fig. 1. Engineering of a Swirling Microvortex Reactor (SMR)

(a,b) CFD simulations of the SMR predicting the mixing efficiency (a) of virtual nanoparticles within the swirling microvortex flow and (b) at cross-sections along the height of the SMR with varied diameters (1mm, 2mm, and 4mm). (c) Schematic showing the synthesis of lipid-polymer nanoparticles (LPNPs) through swirling microvortex flow of PLGA and Lipid/Lipid-PEG aqueous solutions; Photo of a SMR with two precursor inlets. Scalebar is 5mm. (d) TEM image of synthesized LPNPs. Scalebar is 100nm. (e–g) Size distributions of synthesized LPNPs show the effects of (e) the reactor diameter, (f) PLGA-lipid weight ratio (precursor composition), and (g) Reynolds number (Re) on the average size and uniformity of the NPs.

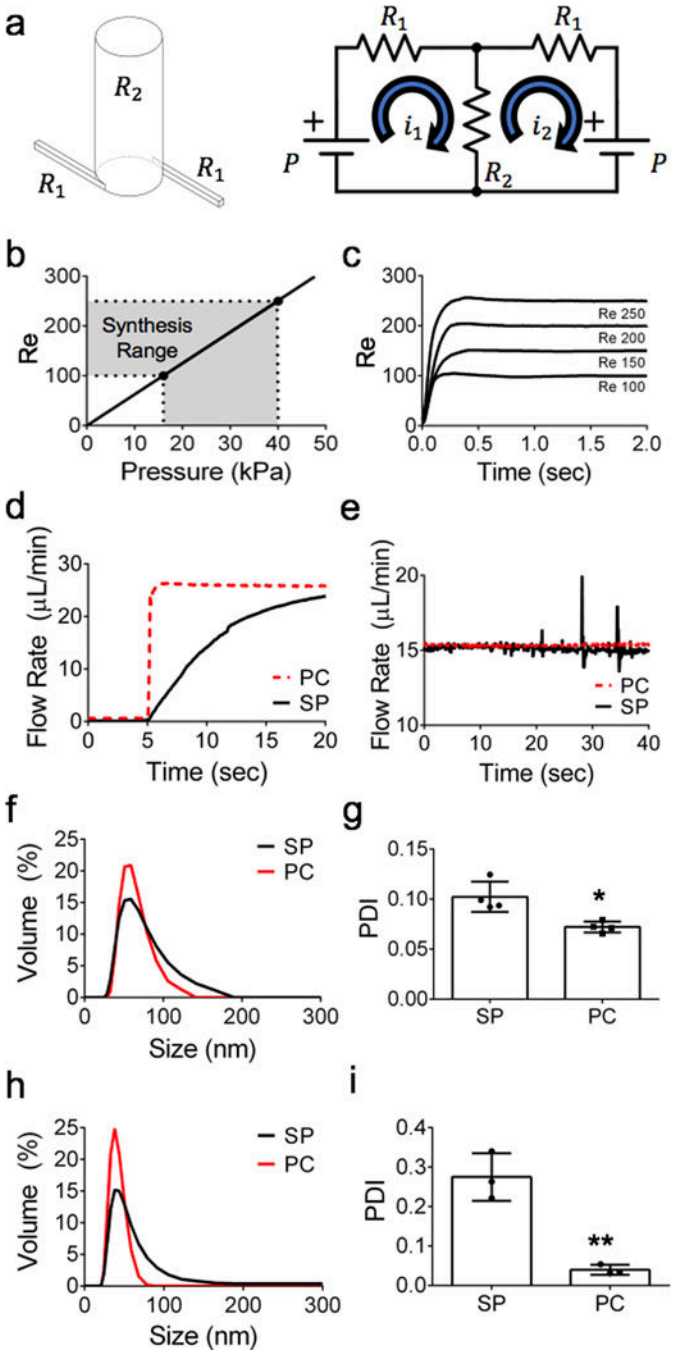

Fig. 2. Integrated SMR with feedback pressure control for LPNP synthesis

(a) Decomposition of the SMR into equivalent fluidic circuit analog for mesh current analysis modelling of the dual pressure control integrated with SMR. Where P represents the inlet pressure of the SMR set by the pressure control system, i_1 and i_2 represent the fluid flow through the system defined by the mesh current analysis method, and R represent the defined resistances of the SMR. (b) Relationship of Reynolds number to the pressure from the mesh current analysis. (c) Control system performance with Reynolds number within the synthesis range. (d, e) Performance of our custom feedback pressure control system (PC) to

syringe pump (SP) for (d) transient and (e) steady-state responses. The size distributions and polydispersity index (PDI) of LPNPs produced for (f, g) the steady-state period of the following 2.5 minutes (n=4; *p=0.0221) and (h, i) the transient period of the beginning 5 seconds (n=3; **p=0.0178). PC is our pressure control system and SP is a commercial syringe pump. Significance was determined by a two-tailed unpaired t-test.

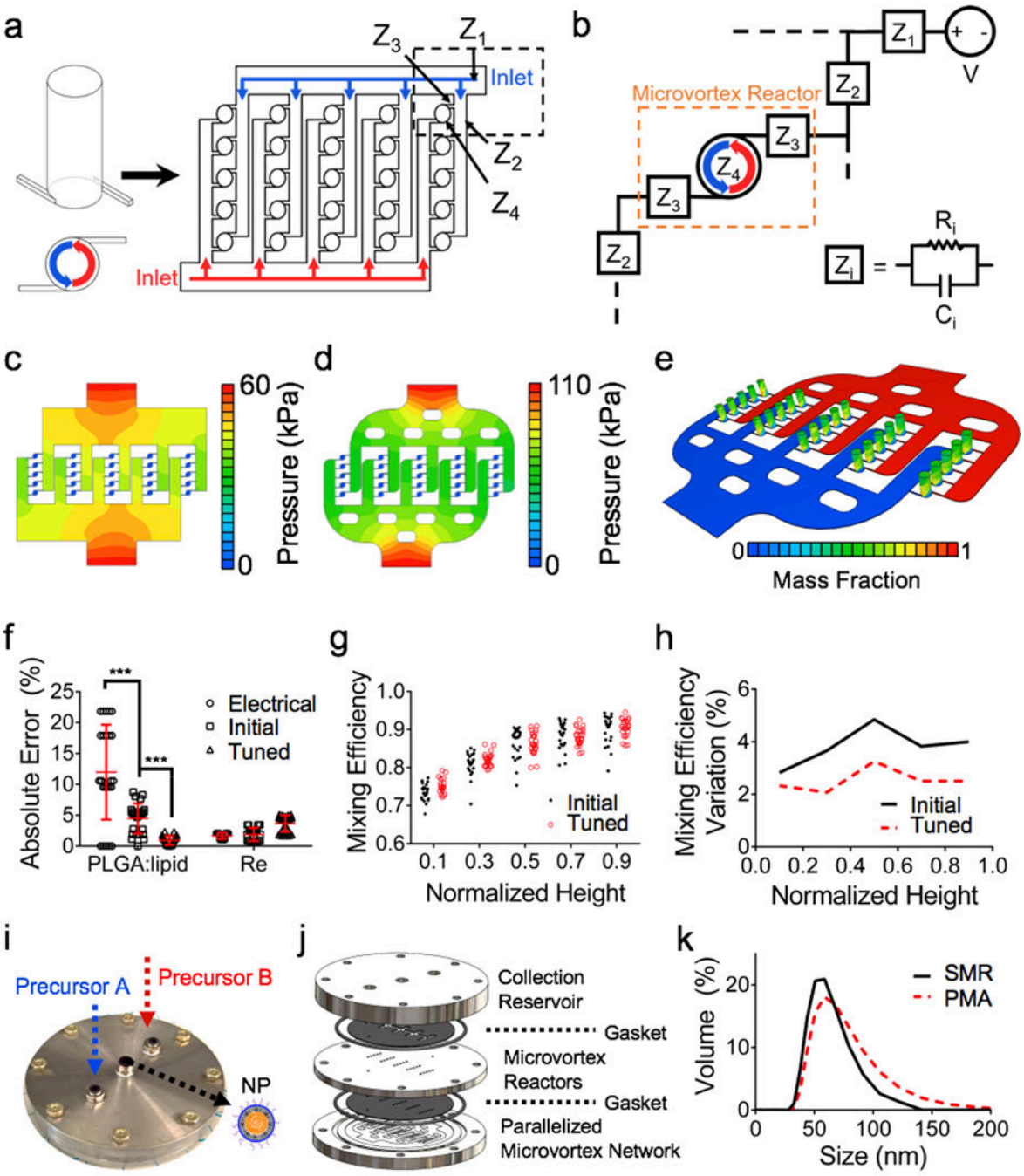

Fig. 3. Development and optimization of a parallelized microvortex array (PMA)

(a) Generalized schematic of our PMA device parallelizing 25 SMRs with a microfluidic network. (b) Fluidic circuit analog decomposition of the PMA network. Z_1 is the impedance of inlet channels connecting all branches of the SMRs. Z_2 is the impedance of the SMR-connecting channels. Z_3 is the impedance of the inlet of the SMR. Z_4 is the impedance of the SMR. (c, d) CFD simulations on pressure distributions of (c) a fluidic and (d) a tuned model of the PMA. (e) CFD simulation predicting a mass fraction distribution of precursor solutions in the finalized PMA. (f) Absolute errors of pressures at the inlets of 25 SMRs in

the PMA for PLGA-lipid ratio and Re for the electrical, initial fluidic, and tuned models (mean ± SEM). (g) Mixing efficiency of 25 individual SMR in the initial fluidic and tuned models. (h) Mixing efficiency variation of the initial fluidic and tuned models. (i, j) Fabricated PMA for NP nanomanufacturing illustrating multitier design consisting of parallelized microvortex network, microvortex reactors, and collection reservoir. (k) Size distributions of synthesized LPNPs using SMR and PMA.

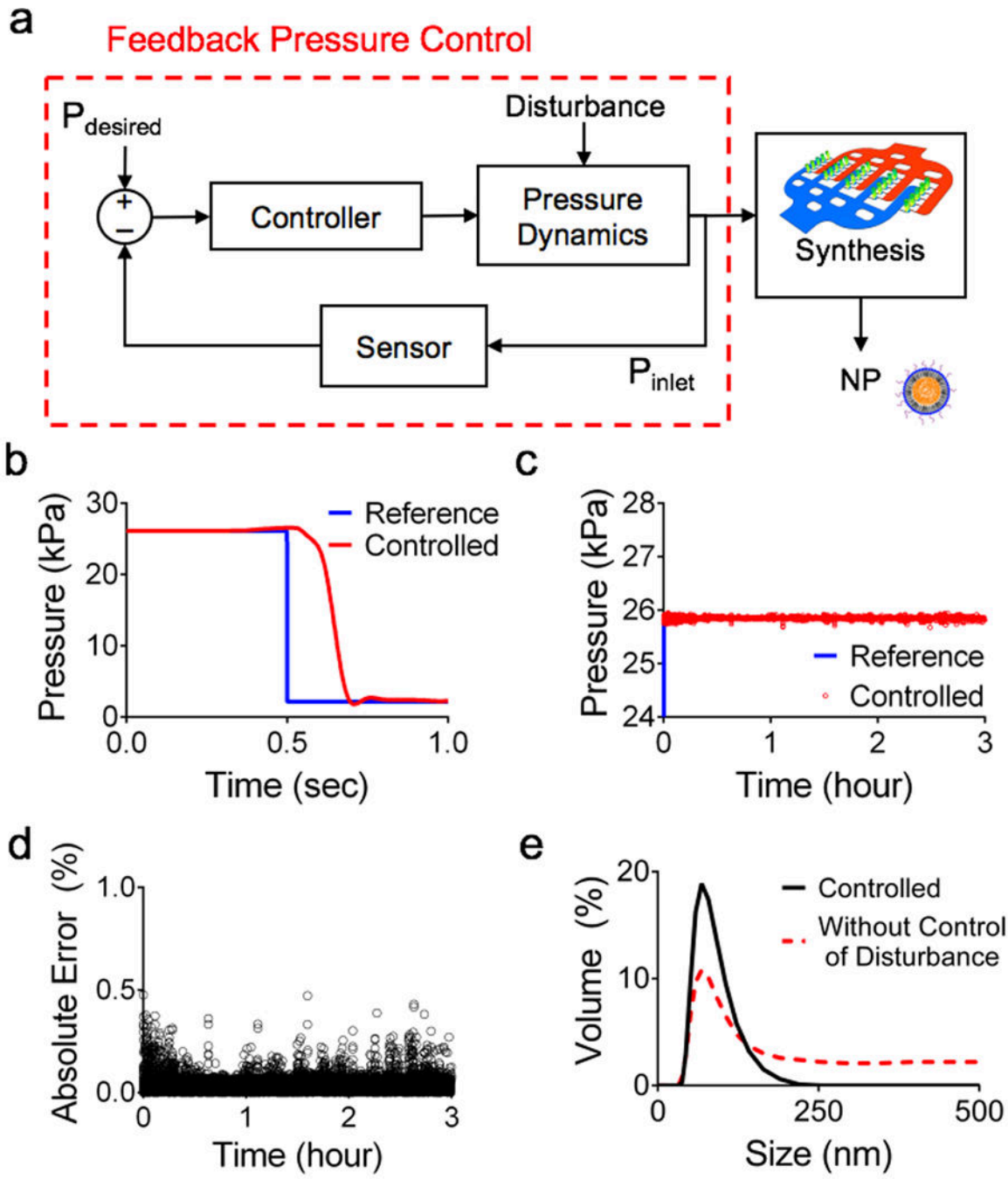

Fig. 4. Integrated PMA for high-precision nanomanufacturing

(a) Schematic of integrated feedback pressure control for LPNP nanomanufacturing on the PMA. (b) Transient response of our custom feedback pressure control system to a step input. (c) Long-term performance of the pressure control system. (d) Absolute error during the long therm pressure control. (e) Size distributions of synthesized LPNPs showing the effect of disturbance mitigation on NP size uniformity.

Table 1

Impedance calculations

The fluidic model impedances Z_{1-4} are given with their corresponding resistances and capacitances used in the calculation.

Resistances (R_i)		Capacitances (C_i)		Impedances (Z_i)	
R_1	9.75E8	C_1	8.22E-12	Z_1	$\frac{1}{8.22E{-}12s + 1.02E{-}9}$
R_2	1.28E9	C_2	8.95E-13	Z_2	$\frac{1}{8.95E{-}13s + 7.78E{-}10}$
R_3	6.08E10	C_3	1.06E-13	Z_3	$\frac{1}{1.06E{-}13s + 1.64E{-}11}$
R_4	1.27E7	C_4	4.16E-12	Z_4	$\frac{1}{4.17E{-}12s + 7.85E{-}8}$